Experimental Eye Research 119 (2014) 44–53

Contents lists available at ScienceDirect

Experimental Eye Research

journal homepage: www.elsevier.com/locate/yexer

Absence of amyloid-beta in lenses of Alzheimer patients: A confocal Raman microspectroscopic study

Ralph Michael [a,b,*], Cees Otto [c], Aufried Lenferink [c], Ellen Gelpi [d], Gustavo A. Montenegro [a], Jurja Rosandić [a], Francisco Tresserra [e], Rafael I. Barraquer [a], Gijs F.J.M. Vrensen [f]

[a] Institut Universitari Barraquer, Universitat Autònoma de Barcelona, Barcelona, Spain
[b] University Eye Clinic, Paracelsus Medical University, Salzburg, Austria
[c] Medical Cell Bio Physics, University of Twente, Enschede, The Netherlands
[d] Neurological Tissue Bank of the Biobanc-Hospital Clinic-Institut d'Investigacions Biomediques August Pi i Sunyer (IDIBAPS), Barcelona, Spain
[e] Department of Pathology, Institut Universitari Dexeus, Barcelona, Spain
[f] Department of Ophthalmology, Leiden University Medical Center, The Netherlands

ARTICLE INFO

Article history:
Received 17 September 2013
Accepted in revised form 26 November 2013
Available online 12 December 2013

Keywords:
cataract
lens
brain
hippocampus
Alzheimer
Raman spectroscopy
amyloid-beta

ABSTRACT

We have compared the protein profiles in plaques and tangles in the hippocampus of post-mortem Alzheimer brains and in opaque and clear regions in the deep cortex of eye lenses of the same donors. From the 7 Alzheimer donors studied, 1 had pronounced bilateral cortical lens opacities, 1 moderate and 5 only minor or no cortical opacities. We focused on beta-sheet levels, a hallmarking property of amyloid-beta, the major protein of plaques and tau protein, the major protein of tangles in Alzheimer brains. Confocal Raman microspectroscopy and imaging was used in combination with hierarchical cluster analysis. Plaques and tangles show high levels of beta-sheets with a beta-sheet to protein ratio of 1.67. This ratio is 1.12 in unaffected brain tissue surrounding the plaques and tangles. In the lenses this ratio is 1.17 independently of the presence or absence of opacities. This major difference in beta-sheet conformation between hippocampus and lens is supported by Congo red and immunostaining of amyloid-beta and tau which were positive for plaques and tangles in the hippocampus but fully negative for the lens irrespective of the presence or absence of opacities. In line with a previous study (Michael et al., 2013) we conclude that cortical lens opacities are not typical for Alzheimer patients and are not hallmarked by accumulation of amyloid-beta, and can thus not be considered as predictors or indicators of Alzheimer disease as claimed by Goldstein et al. (2003).

1. Introduction

In previous papers Goldstein et al. (2003) and Moncaster et al. (2010) described accumulation of amyloid-β (Aβ) in supra-nuclear (cortical) cataracts of patients with Alzheimer disease (AD) and Down syndrome. They conclude from these studies that "The process (i.e. the accumulation of Aβ) that's going on in the brain is also going on in the eye", cited by Gardner (2005). Since then non-invasive *in vivo* ophthalmological methods (quasi-elastic light scatter and fluorescence ligand screening) have been developed by Goldstein and coworkers to identify the presence of Aβ in cortical cataract and advocate its presence as an (early) predictor of AD (Goldstein, 2008; Grohol, 2009).

Because of the paramount clinical importance of this conclusion, we decided to study a large population of cortical cataracts in Alzheimer and non-Alzheimer donors to verify the presence of Aβ in human cataract lenses. Based on histochemical (Congo red and Thioflavin-S staining) and immunohistochemical (Aβ antibody clone 6F/3D) evidence we came to a conflicting conclusion: full absence of Aβ in cortical cataracts in AD and non-AD donors (Michael et al., 2013). In contrast with the Goldstein et al. (2003) and Moncaster et al. (2010) studies we included in our study frontal cortex sections from brain donors with Alzheimer disease as positive controls. The brain slices showed strong positive Congo red staining with a red-to-apple green shift (birefringence) under polarized light, Thioflavin-S fluorescence and positive immunostaining. We discussed this discrepancy at length and have readdressed the question of Aβ in the lens in the present study.

The neuropathology of Alzheimer disease is hallmarked by the presence of amyloid-β plaques and neurofibrillary tangles in the cerebral cortex and hippocampus. As recently reviewed by

* Corresponding author. Institut Universitari Barraquer, Universitat Autònoma de Barcelona, Barcelona, Spain.
E-mail address: ralphm@barraquer.com (R. Michael).

0014-4835/$ – see front matter © 2013 Elsevier Ltd. All rights reserved.
http://dx.doi.org/10.1016/j.exer.2013.11.016

Table 1
Lens opacity findings, donor information and AD classification.

Donor number	Lens circumference affected by cortical opacity[a]	Extension of cortical opacity towards the optical axis[b]	Nuclear cataract[c]	Age	Sex	AD classification neurofibrillary tangles[d]	AD classification neuritic plaques[d]
311a	XXXXX	XXXXX	1	80	f	V	C
311b	XXXXX	XXXXX	1				
321a	XX	XX	2	63	f	V	C
321b	XX	XX	2				
316b	XX	XX	4	91	f	VI	C
316a	X	X	4				
305a	X	X	6	91	m	VI	C
305b	0	0	6				
326a	0	0	4	81	m	VI	C
326b	Not available						
308a	0	0	1	79	f	IV	B
308b	0	0	1				
330a	X	X	2	78	f	V	B
330b	Not available						

Cases collected between May and December 2011.
Hippocampus tissue received from donors 311, 316 and 321.
m: male; f: female.
[a] Degree of lens circumference affected by cortical opacity: 0% = 0; 1–20% = x; 21–40% = xx; 41–60% = xxx; 61–80% = xxxx; 81–100% = xxxxx (100% means entire lens circumference affected.).
[b] Extension of the cortical opacity towards the optical axis is expressed as smallest diameter of a theoretical pupil where the cortical opacity would be visible inside the pupillary area: no cortical opacity = 0; 8.1–10 mm = x; 6.1–8.0 mm = xx; 4.1–6.0 mm = xxx; 2.1–4.0 mm = xxxx; 0–2 mm = xxxxx.
[c] Nuclear cataracts graded in a combined scale for opacity and coloration scales from 0 to 10.
[d] AD classification from brain autopsy, based on neurofibrillary tangles (stages I–VI) according to Braak et al. (2006), and based on neuritic plaques (scores A–C) according to Mirra et al. (1991).

Friedman (2011) the pathological accumulation of Aβ in the brain is due to the enzymatic cleavage by α, β and γ secretases of Aβ peptides from the amyloid precursor protein (APP). Most common are the $Aβ_{1–40}$ and $Aβ_{1–42}$ peptides against which most of the immunohistochemical antibodies are raised. These monomeric peptides are normally broken down by the ubiquitin-proteasome pathway or by phagosomes and lysosomes (Forman et al., 2004). In old age, however, this breakdown is inhibited and the monomeric peptides tend, for unknown reasons, to aggregate to oligomers and eventually to polymers which form amyloid fibrils. These fibrils are molecularly characterized by their regularly aligned β-pleated sheet configuration and form the main components of the plaques in AD. Tau is a neuronal microtubule-associated protein whose expression is strongly up-regulated during neuritogenesis (von Bergen et al., 2006). Upon aging the originally unfolded random coil tau protein is altered by several processes and forms fibrils with a regularly aligned β-pleated sheet configuration (von Bergen et al., 2005). The tau fibrils, localized in the neuronal cytoplasm, are the main components of the tangles which, as the Aβ plaques, obstruct the normal function of the neurons involved.

Although most proteins, including lens crystallins, have β-sheets as part of their molecular conformation, the Aβ peptides in plaques and tau in tangles in AD brains are hallmarked by a high occurrence of these β-sheets (Koudinov et al., 1999) which are present as fibrils. In the present study we have analyzed the molecular conformation of the proteins in plaques and tangles in the hippocampus of neuropathologically verified Alzheimer donors and in the lenses of the same donors using Raman microspectroscopy and imaging. Raman microspectroscopy is a sensitive quantitative analytical method to detect specific molecular conformational bonds in proteins. The protein amide bands in the spectral fingerprint regions around the vibrational bands 1250 cm^{-1} (Amide III) and 1670 cm^{-1} (Amide I) reflect the presence and the amount of α-helical and β-pleated sheet conformations in proteins and thus are appropriate to analyze possible differences between Aβ in AD plaques and the crystallins in the eye lens. In previous studies in human lenses we have shown that the method indeed enables detection of local conformational changes in proteins and lipids and in water content and of local accumulations of these macromolecules. The use of a confocal scanning Raman set up further enables the imaging of these changes and to correlate them with local differences in the (ultra)structure of the lenses but also in individual cells and other tissues (Duindam et al., 1998; Siebinga et al., 1991, 1992; Uzunbajakava et al., 2003a; Uzunbajakava et al., 2003b; van Manen et al., 2008).

Apart from a monolayer of epithelial cells at the anterior pole and developing fibers in a small equatorial zone the lens is a homogenous tissue mainly consisting of mature fibers filled with a high density (30–40%) of specific proteins (mainly α, β and γ crystallins) surrounded by membranes. In the vast majority of mature lens fibers organelles are absent. This means that Raman imaging over extended areas in several regions of the eye lens tissue enables to draw conclusions on the local differences in protein content and molecular conformation. In contrast, brain tissue is a rather in-homogenous tissue with neuronal, astrocytic, oligodendrocytic and microglial cell bodies, vessels, and neuropil consisting of dendrites, axons and cellular processes of glial cells.

The aim of this study was to analyze the differences between hippocampus and lens regarding the hallmarking β-sheet configuration of Aβ. In order to observe potential local differences in brain tissue, we adopted Raman imaging. In the case of plaques and tangles, which are mostly smaller than the imaged area, specific Raman information related to the chemical composition will reflect structural information based on Raman contrast. The extensive Raman data sets typically consisting of 4096 spectra from areas of 900 $μm^2$ were analyzed with hierarchical cluster analysis (HCA). This method combined with Raman imaging data matrices visualizes regions in the tissues with high Raman spectral similarities. For a correct comparison between lens and brain tissue we have used HCA applied to data sets of both tissues.

2. Material and methods

Brain and eye tissue from seven donors was provided by the Neurological Tissue Bank of the Biobank-Hospital Clinic-IDIBAPS (NTB-IDIBAPS), Barcelona in collaboration with the Banco de Ojos para Tratamientos de la Ceguera, Barcelona. Written informed consent for removal of the brain and the eyes for diagnostic and

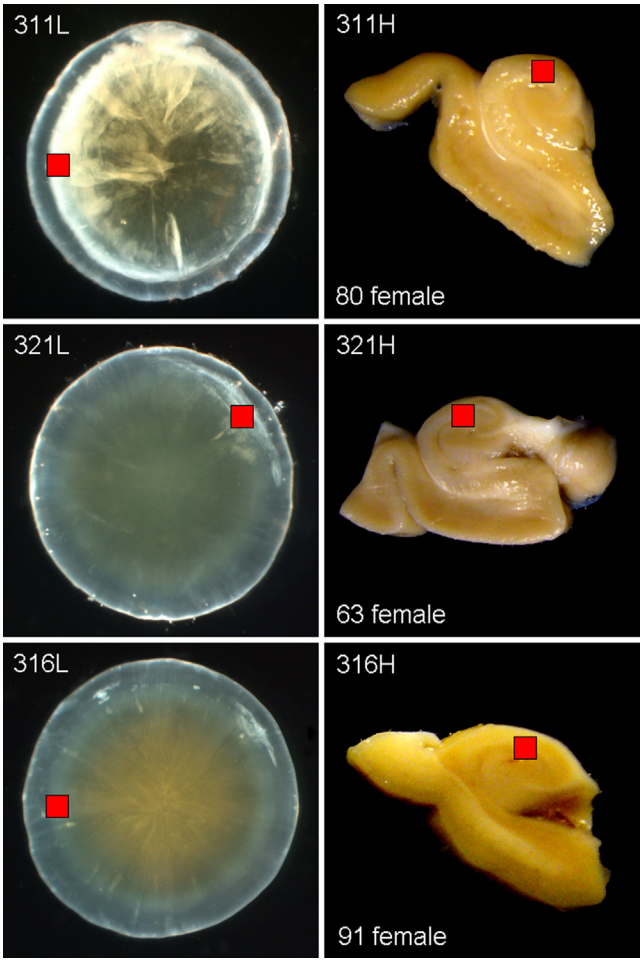

Fig. 1. Dark field images of 3 lenses and the hippocampus tissue of the same donors. The location of the samples analyzed by Raman are indicated.

research purposes were obtained from patients and/or relatives. The research adhered to the tenets of the Declaration of Helsinki on research involving human subjects.

Neuropathological studies of the seven donors were performed at the NTB-IDIBAPS, Barcelona. AD staging was based on neurofibrillar pathology according to Braak et al. (2006) with stages ranging from I to VI and on neuritic plaque score according to CERAD (Mirra et al., 1991) ranging from A to C (Table 1). For this study, hippocampus from 3 donors and lens tissue from all 7 donors were used.

Cortical cataracts were graded for percentage of lens circumference affected by cortical opacities and their extension from the lens periphery towards the optical axis. Nuclear cataracts were graded in a combined scale for opacity and coloration on a scale between 0 and 10. The grading was performed by three different ophthalmologists, and the mean values are given in Table 1.

Lenses were analyzed about 900 μm below the lens capsule, where the cortical opacities are usually located (Michael et al., 2008), and the hippocampi were measured in the CA1 regions (Fig. 1). Lens and hippocampal tissue were fixed in 4% paraformaldehyde in 0.08 M cacodylate buffer (pH 7.3) for maximal one week and then stored in 0.2% paraformaldehyde in 0.08 M cacodylate buffer (pH 7.3) for 5 weeks. One lens half and a piece of the hippocampus was embedded in paraffin and cut in 8 μm thick sections. The sections were stained with Congo red according to Puchtler (Bely and Makovitzky, 2006) and for amyloid-β immunohistochemistry with mouse monoclonal amyloid-β antibody at a dilution 1:50 using clone 6F/3D (NCL-B-Amyloid, Novocastra Labs, Leica Microsystems, Wetzlar, Germany) (Michael et al., 2013). Remaining lens and hippocampal tissue were cut with a Vibratome (Leica 1000S) in slices of 500 μm thickness for the lens and of 50 μm thickness for the hippocampus at the same time and stored in PBS for Raman analysis. Raman analysis was carried out within one week after slicing.

Non-resonant Raman spectroscopy and imaging experiments were performed on a previously described laser-scanning confocal Raman microspectrometer (Pully et al., 2010). The system consist of a Krypton laser (Innova 90-K; Coherent, SantaClara, CA, λ_{exc}647.1 nm), an upright microscope BX41 from Olympus with an objective Olympus, Plan Apochomat, 40×, 0.95NA, coverslip corrected for illumination of the sample as well as for collection of Raman scattered photons. The home-built spectrograph was optimized for broadband (+20 to −3670 cm^{-1}) high-wave number-resolution (1.85–2.85 cm^{-1}/pixel) Raman microspectroscopy. Imaging experiments were performed by raster-scanning the laser beam over a region of interest with a step size of approx. 0.5 μm (30 × 30 μm containing 64 × 64 spectra) with a dwell time per pixel of 50 ms. A full image of each area was thus acquired in ~205 s with a laser power of 35 mW. The measured Raman data were corrected by standard procedures for cosmic ray removal and of pixel-to-pixel variation versus a calibrated light source. Noise in the resulting 3D (spatial × spatial × spectral dimension) data matrix of 4096 spectra times 1600 frequencies was reduced by singular value decomposition (Uzunbajakava et al., 2003a). In three areas of the

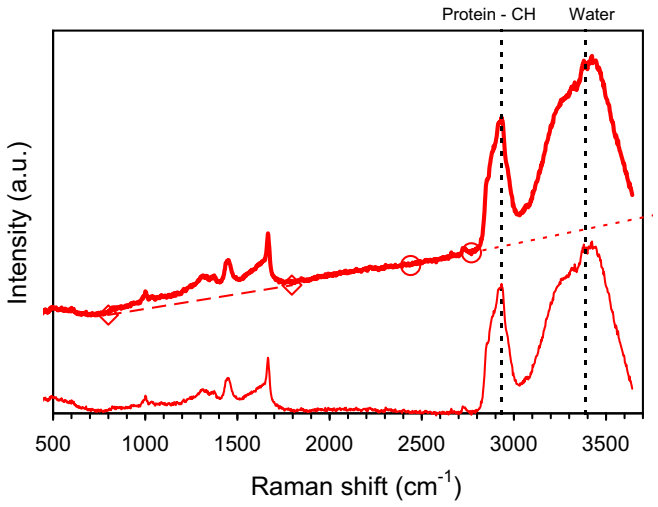

Fig. 2. Uncorrected Raman spectrum from hippocampus (bold red line). The points used for background correction are indicated. The thin line represents the spectrum corrected for background. Raman peaks indicated: 2935 cm^{-1} CH-stretch of proteins and 3390 cm^{-1} water used for protein normalization and estimation of protein concentration.

lens tissue and three areas of the corresponding hippocampal tissue of seven donors Raman data sets were acquired totaling altogether more than 172 thousand (42 × 4096) Raman spectra.

Hierarchical cluster analysis (HCA) was performed on Raman imaging data matrices to visualize regions with high Raman spectral similarities within the 30 × 30 μm samples. In the cluster analysis routine scores derived from principal component analysis were taken as input variables, squared Euclidean distances were used as distance measure, and Ward's algorithm was employed to partition Raman data sets into clusters (van Manen et al., 2005). In the present study we have chosen 4 levels cluster analysis since it most clearly visualizes the local differences in the hippocampal slices. Four different colors were assigned to these 4 clusters.

Background Raman signal was removed by subtracting a linear function. For the so-called fingerprint region (700–1800 cm^{-1}), this function was obtained by a linear fit through the intensity at 800 cm^{-1} and at 1830 cm^{-1}. For the high frequency region (2700–3700 cm^{-1}), this function was obtained by a linear fit through the intensity at 2440 cm^{-1} and at 2770 cm^{-1} (Fig. 2). Protein concentration was calculated according to Huizinga et al. (1989) from the background corrected ratio of the Raman peaks at 3390 cm^{-1} (water) and 2935 cm^{-1} (CH-stretch of proteins). Protein and lipid conformations were analyzed in the fingerprint region after background correction and normalization for protein content. The objective of this study was the analysis of the difference between hippocampus and lens regarding the hallmarking β-sheet configuration of Aβ. For this reason we used the ratio of the Amide I peak at 1668 cm^{-1} (β-sheet) and the protein/lipid peak at 1450 cm^{-1} as a relative measure of the β-sheet content.

3. Results

Donor characteristics and AD staging are summarized in Table 1. From the 7 Alzheimer donors studied, 1 had pronounced bilateral cortical lens opacities, 1 moderate and 5 only minor or no cortical opacities. Immunohistochemical and Congo red observations on the lenses and hippocampi studied (Fig. 3) corroborated the observations described earlier (Michael et al., 2013). The lenses were characterized by the absence of Aβ immunostaining in cataractous and non-cataractous cortical regions of the *post-mortem* donors with Alzheimer disease. In line with previous observations in the frontal cortex of AD brains, hippocampal sections showed congophilic and Aβ positive structures representing amyloid plaques, and tau positive and partially congophilic neurofibrillary tangles (Michael et al., 2013).

In Fig. 4 the results of the 4-cluster analysis of 3 hippocampal slices and 3 deep cortical regions of the lenses of the same AD patients are shown (Fig. 4). The cluster spectra are shown for the fingerprint region (700–1800 cm^{-1}) and the high frequency region (2700–3700 cm^{-1}). The white light gray scale images and false color coded images of the fingerprint region are shown annex to the spectra. Nearly identical fingerprint spectra over the whole scanned area were characteristic for lenses with minor intensity differences in the 4-clusters (Fig. 4). This means that the cluster based color coded images of the lenses reflect only minor differences in local protein conformation and/or protein content. This was confirmed by calculating difference spectra which revealed that the changes in the optical spectra were not related to Raman resonances but were due to baseline variations which may result from spatial variations of fluorescent minority species in the sample. The results of the other 4 lenses studied (not shown) were very similar irrespective of the presence or absence of opacities. The high frequency spectra also showed a great similarity between the 4 clusters within the individual lenses indicating that there are only minor local differences over the scanned area in protein and water content: peaks at 2935 cm^{-1} (CH-stretch of proteins) and 3390 cm^{-1} (water) respectively. The spectra from the cluster analysis in the high frequency range (2700–3650 cm^{-1}) of the hippocampal slices (Fig. 4) revealed that in the scanned areas there were components with substantially different 2935 cm^{-1}/3390 cm^{-1} ratios. For the red and black spectra this ratio is close to that in the lens slices. The blue and green spectra have much lower ratios indicating that these areas have much lower protein. The color coded images show that these high protein areas are well delineated suggesting they are reflecting specific high protein features in rather homogenous regions with low protein content. The most likely, if not only, candidates for these high protein features are the plaques and tangles common in the hippocampal slices as seen in Fig. 3D.

Since we are not yet able to distinguish between plaques and tangles we will use the term "feature" for these high protein regions in this paper. In some instances the location of the features can be traced back in the white light images (v). In the fingerprint region, the hippocampal slices show remarkable peak differences with the lens and additionally remarkable high background signals in the high protein regions (red and black spectra). In the low protein regions (green and blue) the Raman signal is low and only small peaks for protein and lipids at 1450 cm^{-1} and amide I at 1668 cm^{-1} are seen. In the high protein features the intensity of the peaks at 1450 cm^{-1} and the 1668 cm^{-1} are more pronounced. A difference between the lens spectra and hippocampal feature spectra is the substantial higher intensity of the 1668 cm^{-1} as related to the 1450 cm^{-1} peak in the hippocampus. Because the amide I peak at 1668 cm^{-1} reflects the β-sheet configuration of proteins it can tentatively be concluded that the feature regions must contain proteins with a substantially higher β-sheet content than the surrounding tissue and also higher than in the lens.

Another striking difference between lens spectra and hippocampus feature spectra is the absence of well-defined peaks in the hippocampus fingerprint spectra. This may be partly due to the high background in the hippocampus features. When corrected for background the difference remains pronounced (Fig. 5). Striking are the absence of the tyrosine (Ty) and tryptophan (Tr) peaks between 750 and 900 cm^{-1} and between 1550 and 1625 cm^{-1} and the low phenylalanine peak at 1002 cm^{-1}. For full details of Raman assignments the reader is referred to the general Raman literature on this and to the lens papers by

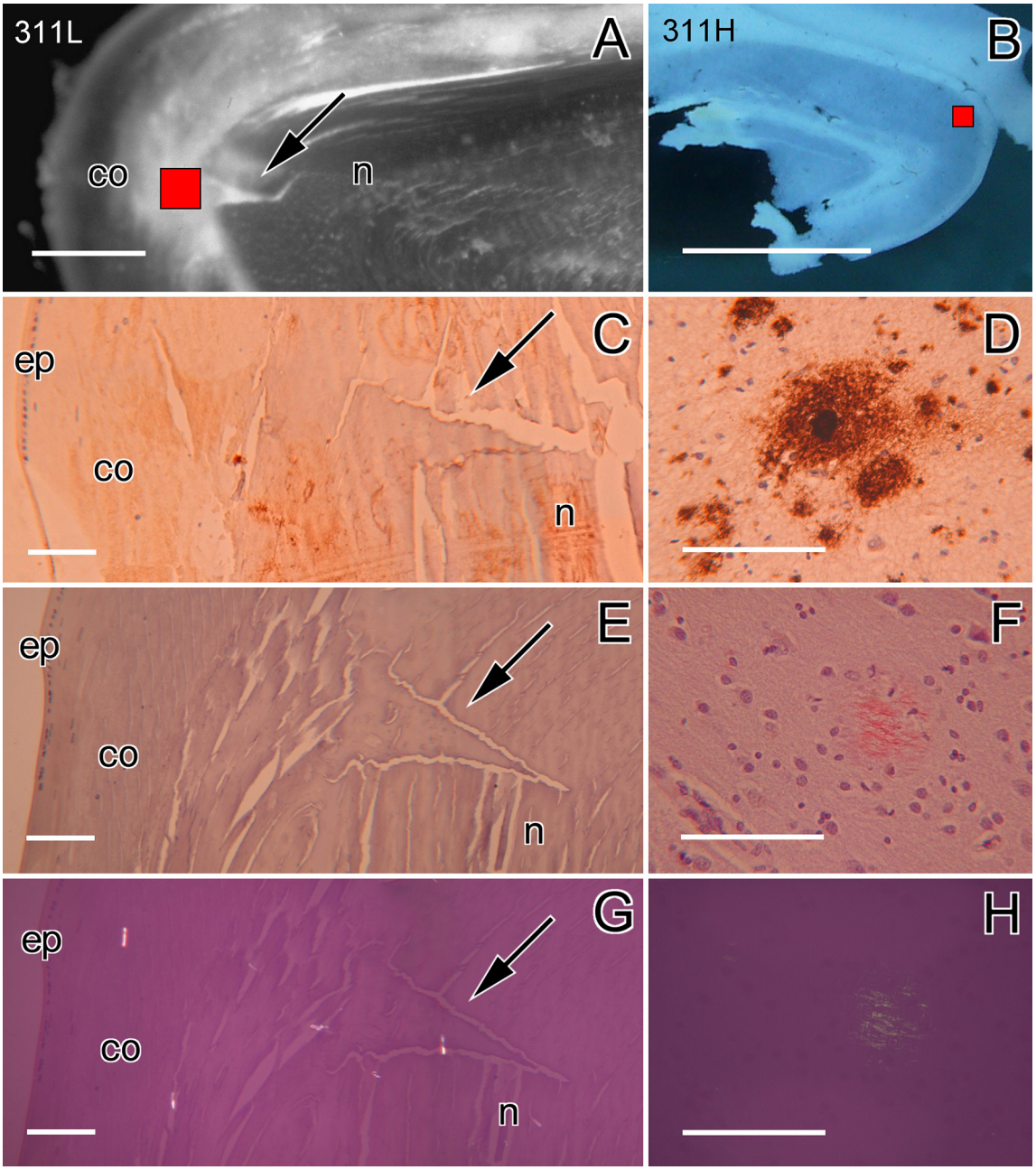

Fig. 3. Examples of tissue slices from lens (A) and hippocampus (B) as prepared for histology and Raman microscopy. Location of the sites for Raman analysis is indicated in red squares. Bright field images of lens and hippocampus sections after immunostaining (C, D), Congo red staining of lens and hippocampus sections in bright field (E, F) and cross-polarized light (G, H) microscopy. Arrows in the lens sections indicate a triangular structure as frequently seen inside cortical opacities (A). The same structure is seen in the histological section, indicating that the studied area is indeed covering the region with the cortical opacity (C, E, G). Some dust particles are purposely left (G) to show that the polarizer setting was indeed in the position to produce apple-green birefringence. Scale bar represents 500 μm (A), 5000 μm (B) and 100 μm (C–H); ep = epithelium, co = cortex, n = nucleus.

Siebinga et al. (1991, 1992). Since lenses and hippocampal features have a comparable protein content this difference must be either due to conformational differences in proteins or to unknown molecular interactions in the hippocampus features influencing the Raman signals.

A striking observation in the cluster data presented in Fig. 4 is that hippocampus features (spectra in red and black for 311H, 321H and 316H) have substantially higher amide I bands around 1668 cm^{-1} than the surrounding brain tissue and the lens indicating that the hippocampus features might have substantially higher β-sheet contents. The mean of all 4096 spectra was taken for the lens and the mean of the spectra corresponding to the features in the hippocampus (highest spectra in red in Fig. 4) and the mean of the surrounding tissue (lowest spectra in blue). Raman background was removed and the spectra were normalized to the protein peak at 2935 cm^{-1} which exclusively reflects the CH-stretch of proteins.

In Fig. 6 (upper part), the averaged normalized spectra of hippocampus features and surrounding tissue are compared. The differences are substantial. In Table 2 we have summarized the

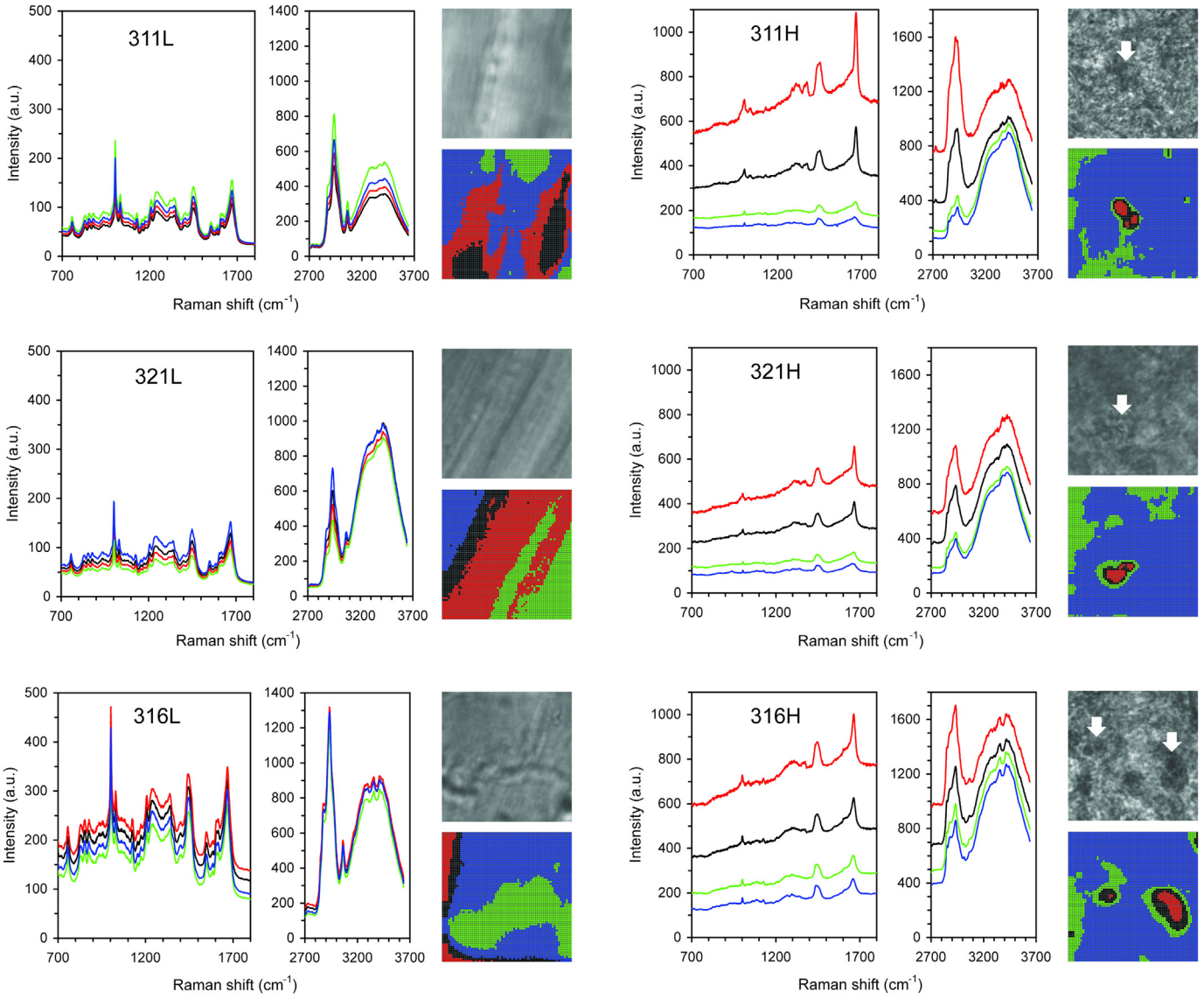

Fig. 4. Hierarchical 4 cluster analysis in the fingerprint (700–1800 cm^{-1}) and high frequency (2700–3700 cm^{-1}) Raman shift region of three lens slices (left panels 311L, 321L, 316L) and three hippocampal slices (right panels 311H, 321H, 316H) of the same post mortem donor. A white light gray scale image of the Raman scan area is given at the upper right of each Raman spectra diagram. A color coded image of the Raman scan area is given at the lower right of each Raman spectra diagram. The colors were assigned from the cluster analysis, which grouped all 4096 local spectra into 4 groups according to similarities. Therefore, the colors reflect local differences in Raman spectra across the scan areas. For instance, the red Raman spectra is found at locations colored in red, the black Raman spectra is found at locations colored in black, and so forth. Note that the color shifts in the lens slices only reflect minor differences in Raman intensity. In the hippocampus small islands with high Raman intensity (red and black) are surrounded by regions with low Raman intensity (green and blue). These islands can be traced back in the white light images (indicated with an arrow head). The scanning area size is 30 × 30 μm and their location inside the tissue is given in Fig. 1.

relative β-sheet content (1668/1450 cm^{-1} ratio), the water/protein ratio (3390/2935 cm^{-1}) and the protein content of the 3 individual hippocampus samples and of the 7 lenses. The ratios of 1668 cm^{-1}/1450 cm^{-1}, reflecting the β-sheet content, are substantially different; 1.67 for the features and 1.12 for the surrounding tissue. The protein content, calculated according to Huizinga et al. (1989) from the 3390/2935 cm^{-1} ratio, is 33.2% and 13.7% respectively (Table 2). In Fig. 6 (lower part), the averaged normalized spectra for hippocampus features and lens deep cortical sites are compared and reveal 1668 cm^{-1}/1450 cm^{-1} ratios of 1.67 and of 1.17 respectively. The averaged protein contents are 33.2% and 34.1% respectively. Further notice that after correction for protein using the 2935 cm^{-1} peak the low frequency peaks at 1450 cm^{-1} for hippocampus features and the lens are not identical. This is in line with common Raman knowledge that the 1450 cm^{-1} peak in addition to protein also reflects lipid components. The peak height difference between hippocampus feature and lens is about 2 indicating that the features may contain 50% lipid components.

4. Discussion

In this study, we have compared the β-sheet content in human lens and hippocampus material from brain donors with neuropathologically confirmed Alzheimer disease using confocal Raman microspectroscopy. We observed a much more pronounced intensity difference between the protein and β-sheet peak in the hippocampal plaques and tangles than in the lens. Moreover, in the deep cortical lens regions (clear or opaque) there proved to be no

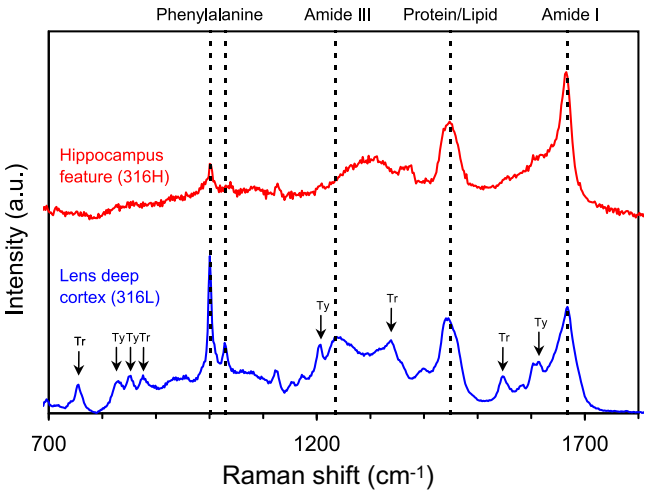

Fig. 5. Representative single Raman spectra in the fingerprint region taken from the cluster analysis of donor 316 (Fig. 4). The red line is the spectrum of the large hippocampal feature (cf. Fig. 4: 316H) and the blue line of the lens. Both spectra are corrected for background. Note the well-defined peaks in the lens and the undefined spectrum of the hippocampus except for the protein/lipid peak at 1450 cm^{-1} and the amide I peak at 1668 cm^{-1}. For clarity the spectra are shifted with respect to intensity. Raman peaks indicated: 1002 cm^{-1} and 1030 cm^{-1}phenylalanine, 1235 cm^{-1} Amide III (α-helix/β-sheet), 1450 cm^{-1} Protein/Lipid (CH2/CH3), 1668 cm^{-1} Amide I (β-sheet), Tr: tryptophan, Ty: tyrosine.

difference in the 1668 cm^{-1}/1450 cm^{-1} ratio (or β-sheet content of proteins) between lenses with or without opacity indicating that cataract changes are not accompanied by changes in β-sheet configuration of the crystallins.

In a previous study using classical staining procedures for Aβ, i.e. Congo red, Thioflavin-S and an antibody against $Aβ_{1–42}$, (Michael et al., 2013) we found also no signs of staining in supranuclear (cortical) cataracts of post mortem donors with AD, and were thus unable to confirm the observations of Goldstein et al. (2003) that cataractous supranuclear regions in lenses of AD donors contain substantial amounts of Aβ.

As outlined in the introduction plaques and tangles in hippocampus and cerebral cortex of AD brains are hallmarked by accumulation of oligomers and fibrils of Aβ and tau protein respectively. These protein species are molecularly characterized by an abundance of regularly organized β-pleated sheets in parallel and anti-parallel orientation (around 58%, (Koudinov et al., 1999)). There is ample evidence (Frid et al., 2007; Prento, 2009) that Congo red and Thioflavin-S intercalate with parallel and anti-parallel oriented β-pleated sheets. This specific interaction is responsible for the dense staining of the fibrils in plaques and tangles in AD brains. For this reason Congo red and Thioflavin-S are used as classical stains for the neuropathological diagnosis of AD. Fourier transform infrared spectroscopy (FTIR) (Lamba et al., 1993) and circular dichroism (Mills et al., 2007; Siezen and Argos, 1983) revealed that isolated α, β and γ-crystallins, forming the most abundant proteins in the lens, fold predominantly in β-pleated sheets (41–68%) and have few α-helical domains (5–12%). It further proved that the α and γ crystallins have substantial high amounts of turns of 19–26% and β-crystallin even up to 40% giving the crystallins a stable tertiary structure (Lamba et al., 1993). In situ the β-sheet amounts of the crystallins is substantial higher (75%) due to differences in protein composition and packing due to the high protein content (30–35%) of the main lens body (Lamba et al., 1993). There is ample evidence that under non-physiological conditions β and γ-crystallins can form fibrils *in vitro* (Fatima et al., 2010; Meehan et al., 2004; Moran et al., 2012; Wang et al., 2010). The $Crygb^{nop}$ mutant of γ-crystallinis forms fibrils *in vivo* in the cell nuclei of primary lens fibers in early development (Sandilands et al., 2002). Papanikolopoulou et al. (2008) showed that *in vitro* formed γ-crystallin fibrils stain positive with Congo red. This implies that the lens crystallins, Aβ and tau protein have comparable properties regarding abundance of β-pleated sheets and their ability to form fibrils. However *in vivo* no signs of fibrils have been found in the cortex and nucleus of aging human lenses (Al-Ghoul et al., 1996; Al-Ghoul and Costello, 1996). This explains why in lens sections no Congo red or Thioflavin staining is observed despite the presence of substantial amounts of β-sheets.

Raman microspectroscopy is a sensitive quantitative analytical method to detect specific molecules and conformational bonds in proteins, lipids and other macromolecules. Peaks and bands in the region between 700 and 1800 cm^{-1} are rather characteristic for e.g. proteins, lipids, DNA and cholesterol (Bergner et al., 2012). In view of the β-sheet hallmarking of Aβ, tau protein and crystallins, the fingerprint peak around 1668 cm^{-1} (Amide I) is of special interest since it reflects the presence of β-sheet conformations in proteins. The band around 1450 cm^{-1} reflects the CH- vibration mode of proteins and lipids and can be considered as a good relative measure for the protein and lipid content of a tissue. Since lens fibers are mainly composed of proteins and have a remarkably low overall lipid content of about 4% in the cortex and about 2% in the nucleus (Li et al., 1985) the 1450 cm^{-1} peak actually reflects the protein content of lens fibers. Therefore the 1668 cm^{-1}/1450 cm^{-1} ratio can be considered as a reliable estimate of the relative contribution of β-sheets to the structure of the crystallins. For plaques and tangles in the brain the situation is different since studies have shown that plaques contain in addition to Aβ and tau fibrils an about equal amount of cholesterol and lipids (D'Errico et al., 2008; Panchal et al., 2010). The 2935 cm^{-1} peak only reflects the CH stretch of proteins. The observation that the 1450 cm^{-1} peak is nearly twice as high in the hippocampal features than in the lens, when corrected for protein content using this 2935 cm^{-1} peak, corroborates the high lipid and cholesterol content of plaques and tangles. Additionally to these differences, we see that brain tissue exhibit a considerable amount of background (Fig. 4: 311H, 321H 316H). This has been earlier observed by Hanlon et al. (1999) who termed it brain tissue auto-fluorescence. Interestingly we note that an increase in the amplitude of the hippocampus tissue auto-fluorescence correlates with the location of the features.

As described under results the cluster analysis reveals that the intensity difference between the protein and β-sheet peak is much more pronounced in the hippocampal plaques and tangles than in the lens. When corrected for auto-fluorescence background and protein content (Fig. 6) the ratio 1668 cm^{-1}/1450 cm^{-1} can be considered as an estimate of the relative differences in β-sheet content of proteins in hippocampal features and lens. In the lens the mean 1668 cm^{-1}/1450 cm^{-1} ratio is 1.17 and in the hippocampal plaques and tangles 1.67. In view of the presence of cholesterol and lipids in the plaques and the fact that cholesterol has a 1668 cm^{-1}/1450 cm^{-1} ratio of 0.50–0.55 (Baraga et al., 1992; Bergner et al., 2012) and the lipid triolein of 0.56 (Baraga et al., 1992) the value of 1.67 for the hippocampal features is an underestimation of the real relative contribution of Aβ to the β-sheet ratio of plaques and tangles. If we conservatively take a content of cholesterol and lipids in plaques and tangles of about 50% (previous paragraph) and a mean 1668 cm^{-1}/1450 cm^{-1} ratio of 0.55 for lipid and cholesterol, the relative β-sheet contribution of these latter molecules to the β-sheet ratio in the features is $0.5 \times 0.55 = 0.275$. The contribution by the proteins is therefore $1.67 - 0.275 = 1.395$. However the proteins, mainly Aβ, make up only 50% of the features. In case the features would consist of Aβ only the 1668 cm^{-1}/

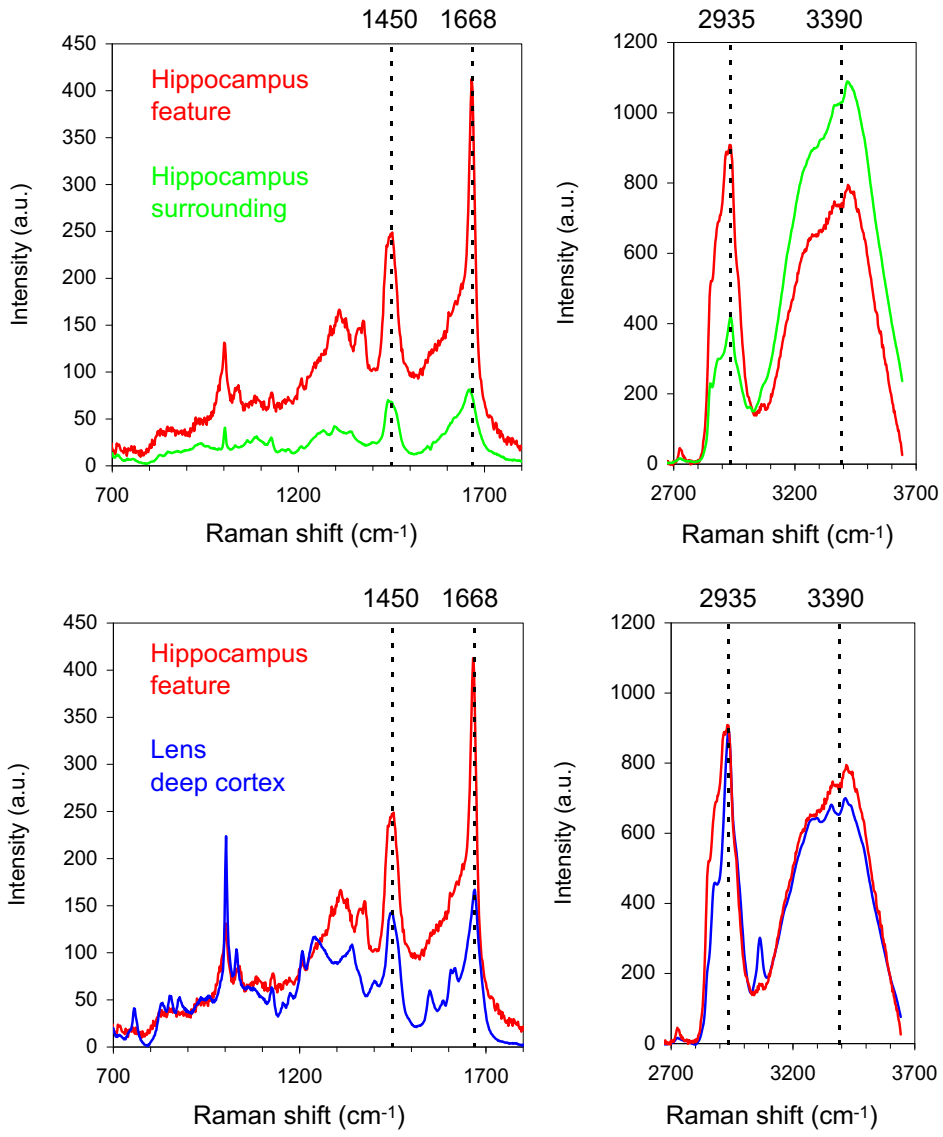

Fig. 6. Averaged spectra of the hippocampus features (red line) and feature surrounding (green line) after correction for background (upper diagrams) and the same averaged spectra of the brain features (red line) compared to the lens slices (blue line) after correction for background and normalized for protein at 2935 cm^{-1} (lower diagrams). Notice the substantial higher Amide I band at 1668 cm^{-1} in the brain feature than in the surrounding. Since this band reflects the β-sheet configuration of proteins and lipids it shows the substantial accumulation of β-sheets in the features as compared to the surrounding. Most remarkable for the features as compared to the lens are the pronounced peaks at 1450 cm^{-1} (protein/lipid) and the Amide I (β-sheets) at 1668 cm^{-1}. Notice the difference of the 1450 cm^{-1} peak between lens and hippocampus feature despite the normalization for protein. Since in the lens the amount of lipids is less than 2% this indicates that in the lens this peak mainly reflects the proteins and that in hippocampus features a considerable amount of cholesterol and lipids must be present.

Table 2
Beta-sheet configuration and protein content in the deep lens cortex and in the hippocampus features and surroundings.

Donor	β-Sheet/protein ratio			Protein/water ratio			Protein content (%)[a]		
	Lens	H-feature	H-surround	Lens	H-feature	H-surround	Lens	H-feature	H-surround
311	1.16	1.89	1.07	0.68	0.52	3.11	34.4	40.7	10.3
321	1.08	1.59	1.09	1.26	1.28	2.77	22.1	21.8	11.4
316	1.11	1.49	1.21	0.56	0.60	1.50	39.0	37.3	19.2
305	1.21			0.69			34.2		
326	1.22			0.81			30.6		
308	1.18			0.63			36.1		
330	1.18			0.48			42.8		
Mean ± SD	1.17 ± 0.05	1.67 ± 0.21	1.12 ± 0.07	0.73 ± 0.26	0.80 ± 0.42	2.46 ± 0.85	34.1 ± 6.6	33.2 ± 10.0	13.7 ± 4.9

For the lens the overall mean of the β-sheet/protein ratio (1668/1450 cm^{-1}) and protein/water ratio (3390/2935 cm^{-1}) of the 30 × 30 μm^2 sample from the individual lenses are taken. For the hippocampus features (H-feature) and surroundings (H-surround) the mean of the highest (red) and lowest (blue) spectra of the 4 cluster analysis (Fig. 4) are taken from the individual samples. Student's *t*-test reveals significant differences at the $p < 0.05$ level for the β-sheet/protein ratio (1668/1450 cm^{-1}) between the hippocampus feature and the lens and hippocampus surrounding. For the protein/water ratio (3390/2935 cm^{-1}) and the protein content a significant difference at the $p < 0.05$ level is revealed between the hippocampus surrounding and the hippocampus feature and lens. Although systematically lower, because of paraformaldehyde fixation, the lens protein content is in line with previous observations (Augusteyn, 2010). The low protein content of the unaffected healthy hippocampal regions is in line with common estimates of the cytoplasm of cells.

[a] Calculated from the water/protein ratio (3390/2935 cm^{-1}) according to Huizinga et al. (1989).

1450 cm^{-1} ratio would be 2 × 1.395 = 2.79. This is about 2.4 times as high as that of the lens crystallins (1.17). Moreover in the deep cortical lens regions (clear or opaque) analyzed in this paper there proved to be no difference in the 1668 cm^{-1}/1450 cm^{-1} ratio between lenses with or without opacity indicating that cataract changes are not accompanied by changes in β-sheet configuration of the crystallins. In contrast the non-affected regions in the hippocampus have a 1668 cm^{-1}/1450 cm^{-1} ratio of 1.12 (Table 2) indicating that the formation of plaques and tangles is accompanied by the accumulation of proteins with a much higher level of β-sheets. That could correspond to tau accumulation in dystrophic neurites around plaques and fine neuropil threads observed in AD tissue. For comparison we have calculated the 1668 cm^{-1}/1450 cm^{-1} ratio of several proteins using the original Raman spectra given in the literature (Table 3). It is well known that β-sheets form an intrinsic conformational part of many if not all proteins. However, lens crystallins have a substantially higher amount of β-sheet conformation as seen in the table. The table also shows that fibrillar molecules as synthetic-Aβ and Aβ in senile plaques have an even higher β-sheet moiety. It can be concluded that confocal Raman spectroscopy and imaging and multivariate analysis methods like hierarchical cluster analysis are sensitive and highly discriminative tools that enable detection of differences in β-sheet conformation to study differences in β-sheets among tissues and locally within tissues.

An unexpected outcome of the present study is the absence in the plaque and tangle spectra of peaks for the aromatic amino acids (aromatic-AA's) tryptophan and tyrosine which are so characteristic for Raman spectra of crystallins (Fig. 5) and of most proteins with a natural preponderance of these amino acids. This is even more unexpected as we have noticed that the hippocampal tissue surrounding plaques and tangles is in good agreement with a typical protein-lipid Raman spectrum. This spectrum is also in good agreement with previously Raman spectra of brain tissue. Moreover, in an amyloid peptide model based on the core sequence of Aβ, the Raman spectrum is rather similar to that of other proteins (Hamley et al., 2010). In addition, the small and broad peak at 1002 cm^{-1}, reflecting the aromatic-AA phenylalanine, is also deviating from the Raman spectra of crystallins and other proteins. This deviation could be due to the absence or a significant lower aromatic-AA's content of Aβ. However this is not supported by knowledge of the primary amino acid sequence. From the known sequence of $Aβ_{1–42}$ it can be calculated that 11.9% of the AA's of this protein are aromatic with a slight preponderance of phenylalanine (Mager, 1998). Sequence analysis of human β and bovine γ crystallins revealed aromatic amino acids contents of 10.2% and 14.4% respectively (Fujii et al., 2011; Norledge et al., 1997). This means that the aromatic-AA's content of Aβ is not significantly different from that of crystallins and most likely also not from other proteins and therefore cannot explain the deviating Raman spectrum of Aβ. As already mentioned *in vivo*, Aβ and tau proteins in plaques and tangles are formed by dense accumulations of fibrils. It can be concluded from the presented data that fibrillar compaction leads to typical Raman spectra of the plaques and tangles, which are different from classical protein Raman spectra and also different from Raman spectra that represent a mixture of lipid spectra and protein spectra, such as from the unaffected brain tissue surrounding the plaques and tangles. Another possibility is that the presence of cholesterol and (phospho) lipids and their close connection with Aβ fibrils in the plaques and tangles may lead to changes in the Raman spectra.

Table 3
Relative contribution of β-sheets in pure proteins, human lens fibers, hippocampal plaques and surrounding brain tissue.

Protein	Ratio[a]	Reference
Collagen	0.61	(Karampas et al., 2013)
Collagen	0.82	(Baraga et al., 1992)
Elastin	0.83	(Baraga et al., 1992)
Albumin	0.82	(Bergner et al., 2012)
α-synuclein	0.58–0.67	(Maiti et al., 2004)
Casein	0.54	(Jarvis et al., 2007)
Insulin	0.89	(Yamamoto and Watarai, 2012)
Insulin amyloid	1.25	(Yamamoto and Watarai, 2012)
Synthetic amyloid β	1.57	(Dong et al., 2003)
Lens crystallins in situ	1.17	(this paper)
Surrounding brain tissue	1.12	(this paper)
Amyloid plaques/tangles	1.67	(this paper)
Amyloid β	2.79	(this paper)
Model amyloid[b]	3.4	(Hamley et al., 2010)

[a] Calculated from the 1668 cm^{-1}/1450 cm^{-1} ratios in the original Raman spectra.
[b] Based on core sequence of Aβ (8 amino acids from which 4 are aromatic).

5. Summary and conclusion

The present confocal Raman microspectroscopic and imaging study, aided by hierarchical cluster analysis, reveals that proteins forming opaque regions in lenses and proteins in hippocampal plaques and tangles in AD donors have significantly different Raman profiles. Especially the Amide I peak of the hallmarking β-sheets is substantially higher (2.4 times) in plaques and tangles. Moreover due to fibrillation and/or co-localization of cholesterol and lipids the Raman peaks for aromatic-amino acids are nearly absent in plaques and tangles.

On account of these observations it seems justified to conclude that amyloid-β and tau protein, the major proteins of the plaques and tangles, are indeed hallmarked by a high β-sheet content as previously described and have accumulated in large amounts in plaques and tangles (Forman et al., 2004; Friedman, 2011; von Bergen et al., 2005). Because the β-sheet content of the cataractous lens proteins is low in comparison with Aβ, it is tempting to conclude that amyloid-β is absent in cortical cataracts. It can be argued, however, that the high β-sheet level in plaques and tangles is due to formation of fibrils which leads to a high local density of amyloid-β and tau protein (Forman et al., 2004; von Bergen et al., 2005) and consequently to high β-sheets peaks. As far as we are aware of, fibrils have not been described in human cortical cataracts. This means that the relative low β-sheet level in the lens could be due to the absence of fibril formation and is not proof of the absence of amyloid-β. In line with this the absence of Congo red and Thioflavin-S staining in lens opacities can also be explained by this absence of fibrils. Absence of staining in lens opacities using an amyloid-β specific antibody, however, is not favoring this point of view. In addition we have not observed significant differences in Raman profiles between opaque and transparent regions in the deep cortical lens cortex of the 7 lenses studied in the present paper. This means that if present at all, amyloid-β in opacities must be present in low concentrations i.e. below the detection level of antibody staining and Raman analysis. This is in line with a point previously discussed (Michael et al., 2013): "that the origin of large amounts of Aβ responsible for the massive Congo red staining in the Goldstein paper is not supported by data in literature on the presence of large amounts of its precursor molecule APP and its breakdown enzymes in the lens".

In conclusion the present Raman observations corroborate our previous histological and immunohistochemical findings (Michael et al., 2013) that cataracts in eye lenses of AD donors do not contain substantial amounts of amyloid-β as was suggested by Goldstein et al. (2003). This strongly suggests that cortical cataract, although it may be comorbid with AD in some cases, has no relation with the main pathological signature of AD i.e. accumulation of amyloid-β and that cortical cataract and AD are therefore not likely

to be causally linked. This also means that cortical cataract cannot be considered as indicator and/or predictor of AD.

Acknowledgment

The authors thank lens and brain donors for their generous donation of tissue for research. We are very grateful to Barbara Liszka (Medical Cell Bio Physics, University of Twente, Enschede, The Netherlands) for operating the Raman setup. We gratefully acknowledge Jeanne Pertijs (Dept. of Pharmacology and Toxicology, Radboud University Nijmegen, The Netherlands) for her excellent preparation of the hippocampal slices. We also acknowledge the technical support of Sara Charif for immunohistochemical studies at the Neurological Tissue Bank of the IDIBAPS Biobank.

References

Al-Ghoul, K.J., Costello, M.J., 1996. Fiber cell morphology and cytoplasmic texture in cataractous and normal human lens nuclei [published erratum appears in Curr Eye Res 1996 Jul;15(7):following 805] Curr. Eye Res. 15, 533–542.
Al-Ghoul, K.J., et al., 1996. Distribution and type of morphological damage in human nuclear age-related cataracts. Exp. Eye Res. 62, 237–251.
Augusteyn, R.C., 2010. On the growth and internal structure of the human lens. Exp. Eye Res. 90, 643–654.
Baraga, J.J., et al., 1992. In situ optical histochemistry of human artery using near infrared Fourier transform Raman spectroscopy. Proc. Natl. Acad. Sci. U. S. A. 89, 3473–3477.
Bely, M., Makovitzky, J., 2006. Sensitivity and specificity of Congo red staining according to Romhanyi. Comparison with Puchtler's or Bennhold's methods. Acta Histochem. 108, 175–180.
Bergner, N., et al., 2012. Unsupervised unmixing of Raman microspectroscopic images for morphochemical analysis of non-dried brain tumor specimens. Anal. Bioanal. Chem. 403, 719–725.
Braak, H., et al., 2006. Staging of Alzheimer disease-associated neurofibrillary pathology using paraffin sections and immunocytochemistry. Acta Neuropathol. 112, 389–404.
D'Errico, G., et al., 2008. Interaction between Alzheimer's Abeta(25-35) peptide and phospholipid bilayers: the role of cholesterol. Biochim. Biophys. Acta 1778, 2710–2716.
Dong, J., et al., 2003. Metal binding and oxidation of amyloid-beta within isolated senile plaque cores: Raman microscopic evidence. Biochemistry 42, 2768–2773.
Duindam, J.J., et al., 1998. Cholesterol, phospholipid, and protein changes in focal opacities in the human eye lens. Invest. Ophthalmol. Vis. Sci. 39, 94–103.
Fatima, U., et al., 2010. Structures of differently aggregated and precipitated forms of gamma B crystallin: an FTIR spectroscopic and EM study. Protein Pept. Lett. 17, 1155–1162.
Forman, M.S., et al., 2004. Neurodegenerative diseases: a decade of discoveries paves the way for therapeutic breakthroughs. Nat. Med. 10, 1055–1063.
Frid, P., et al., 2007. Congo red and protein aggregation in neurodegenerative diseases. Brain Res. Rev. 53, 135–160.
Friedman, R., 2011. Aggregation of amyloids in a cellular context: modelling and experiment. Biochem. J. 438, 415–426.
Fujii, N., et al., 2011. Simultaneous stereoinversion and isomerization at the Asp-4 residue in betaB2-crystallin from the aged human eye lenses. Biochemistry 50, 8628–8635.
Gardner, A., 2005. Eyes might hint at Alzheimer's. HealthDay Reporter. http://news.e-healthsource.com/index.php?p=news1&id=528592.
Goldstein, L.E., 2008. Optics meets Alzheimer's disease: seeing the way to a cure. In: Annual Meeting Optical Society of America: Frontiers in Optics Plenary Session, Monday, Oct. 9 2008.
Goldstein, L.E., et al., 2003. Cytosolic beta-amyloid deposition and supranuclear cataracts in lenses from people with Alzheimer's disease. Lancet 361, 1258–1265.
Grohol, J., 2009. Optics Tests for Early Alzheimer's Diagnosis Make Significant Advances. PsychCentral.com. http://psychcentral.com/news/archives/2006-10/osoa-otf100306.html.
Hamley, I.W., et al., 2010. Alignment of a model amyloid peptide fragment in bulk and at a solid surface. J. Phys. Chem. B 114, 8244–8254.
Hanlon, E.B., et al., 1999. Near-infrared fluorescence spectroscopy detects Alzheimer's disease in vitro. Photochem. Photobiol. 70, 236–242.
Huizinga, A., et al., 1989. Local variation in absolute water content of human and rabbit eye lenses measured by Raman microspectroscopy. Exp. Eye Res. 48, 487–496.
Jarvis, R.M., et al., 2007. Quantification of casein phosphorylation with conformational interpretation using Raman spectroscopy. Analyst 132, 1053–1060.
Karampas, I.A., et al., August 2013. A quantitative bioapatite/collagen calibration method using Raman spectroscopy of bone. J. Biophotonics 6 (8), 573–586.
Koudinov, A.R., et al., 1999. HDL phospholipid: a natural inhibitor of Alzheimer's amyloid beta-fibrillogenesis? Clin. Chem. Lab. Med. 37, 993–994.
Lamba, O.P., et al., 1993. Estimation of the secondary structure and conformation of bovine lens crystallins by infrared spectroscopy: quantitative analysis and resolution by Fourier self-deconvolution and curve fit. Biochim. Biophys. Acta 1163, 113–123.
Li, L.K., et al., 1985. Membrane cholesterol and phospholipid in consecutive concentric sections of human lenses. J. Lipid Res. 26, 600–609.
Mager, P.P., 1998. Molecular simulation of the primary and secondary structures of the Abeta(1-42)-peptide of Alzheimer's disease. Med. Res. Rev. 18, 403–430.
Maiti, N.C., et al., 2004. Raman spectroscopic characterization of secondary structure in natively unfolded proteins: alpha-synuclein. J. Am. Chem. Soc. 126, 2399–2408.
Meehan, S., et al., 2004. Amyloid fibril formation by lens crystallin proteins and its implications for cataract formation. J. Biol. Chem. 279, 3413–3419.
Michael, R., et al., 2008. Morphology of age-related cuneiform cortical cataracts: the case for mechanical stress. Vision Res. 48, 626–634.
Michael, R., et al., 2013. Absence of beta-amyloid in cortical cataracts of donors with and without Alzheimer's disease. Exp. Eye Res. 106, 5–13.
Mills, I.A., et al., 2007. Folding and stability of the isolated Greek key domains of the long-lived human lens proteins gammaD-crystallin and gammaS-crystallin. Protein Sci. 16, 2427–2444.
Mirra, S.S., et al., 1991. The Consortium to Establish a Registry for Alzheimer's Disease (CERAD). Part II. Standardization of the neuropathologic assessment of Alzheimer's disease. Neurology 41, 479–486.
Moncaster, J.A., et al., 2010. Alzheimer's disease amyloid-beta links lens and brain pathology in Down syndrome. PLoS One 5, e10659.
Moran, S.D., et al., 2012. Two-dimensional IR spectroscopy and segmental 13C labeling reveals the domain structure of human gammaD-crystallin amyloid fibrils. Proc. Natl. Acad. Sci. U. S. A. 109, 3329–3334.
Norledge, B.V., et al., 1997. The X-ray structure of a mutant eye lens beta B2-crystallin with truncated sequence extensions. Protein Sci. 6, 1612–1620.
Panchal, M., et al., 2010. Enrichment of cholesterol in microdissected Alzheimer's disease senile plaques as assessed by mass spectrometry. J. Lipid Res. 51, 598–605.
Papanikolopoulou, K., et al., 2008. Formation of amyloid fibrils in vitro by human gammaD-crystallin and its isolated domains. Mol. Vis. 14, 81–89.
Prento, P., 2009. Staining of macromolecules: possible mechanisms and examples. Biotech. Histochem. 84, 139–158.
Pully, V.V., et al., 2010. Hybrid Rayleigh, Raman and two-photon excited fluorescence spectral confocal microscopy of living cells. J. Raman Spectrosc. 41, 599–608.
Sandilands, A., et al., 2002. Altered aggregation properties of mutant gamma-crystallins cause inherited cataract. EMBO J. 21, 6005–6014.
Siebinga, I., et al., 1991. Age-related changes in local water and protein content of human eye lenses measured by Raman microspectroscopy. Exp. Eye Res. 53, 233–239.
Siebinga, I., et al., 1992. Ageing and changes in protein conformation in the human lens: a Raman microspectroscopic study. Exp. Eye Res. 54, 759–767.
Siezen, R.J., Argos, P., 1983. Structural homology of lens crystallins. III. Secondary structure estimation from circular dichroism and prediction from amino acid sequences. Biochim. Biophys. Acta 748, 56–67.
Uzunbajakava, N., et al., 2003a. Nonresonant confocal Raman imaging of DNA and protein distribution in apoptotic cells. Biophys. J. 84, 3968–3981.
Uzunbajakava, N., et al., 2003b. Nonresonant Raman imaging of protein distribution in single human cells. Biopolymers 72, 1–9.
van Manen, H.J., et al., 2005. Single-cell Raman and fluorescence microscopy reveal the association of lipid bodies with phagosomes in leukocytes. Proc. Natl. Acad. Sci. U. S. A. 102, 10159–10164.
van Manen, H.J., et al., 2008. Noninvasive imaging of protein metabolic labeling in single human cells using stable isotopes and Raman microscopy. Anal. Chem. 80, 9576–9582.
von Bergen, M., et al., 2005. Tau aggregation is driven by a transition from random coil to beta sheet structure. Biochim. Biophys. Acta 1739, 158–166.
von Bergen, M., et al., 2006. Spectroscopic approaches to the conformation of tau protein in solution and in paired helical filaments. Neurodegener. Dis. 3, 197–206.
Wang, Y., et al., 2010. Formation of amyloid fibrils in vitro from partially unfolded intermediates of human gammaC-crystallin. Invest. Ophthalmol. Vis. Sci. 51, 672–678.
Yamamoto, S., Watarai, H., 2012. Raman optical activity study on insulin amyloid- and prefibril intermediate. Chirality 24, 97–103.